***Tulp3* quantitative alleles titrate requirements for viability, brain development, and kidney homeostasis but do not suppress *Zfp423* mutations in mice.**

Corinne A. McCoy, Dorothy Concepcion, Mark G. Mezody, Raquel Z. Lara[†], Ojas Deshpande[†], Catherine Liang, Renee Long[†], and Bruce A. Hamilton

Department of Cellular and Molecular Medicine, Department of Medicine, Division of Genomics and Precision Medicine, Moores Cancer Center, and Institute for Genomic Medicine
UC San Diego School of Medicine
La Jolla, CA 92093

[†] Present addresses:
RL: Department of Dermatology, Stanford University School of Medicine, Redwood City, CA 94063
OD: University of Arizona College of Medicine, Phoenix, AZ 85004
RZL: University of Texas, Rio Grande Valley School of Medicine, Edinburg, TX 78541

ORCIDs:
CAM: 0000-0001-8960-414X
DC: 0000-0002-8506-1229
MGM: 0009-0009-0071-9852
RZL: 0000-0003-3769-9313
OD: 0000-0002-6029-2370
CL: 0009-0009-4808-514X
RL: 0000-0003-1638-3459
BAH: 0000-0001-5599-9139

ABSTRACT

Tubby-like protein 3 (TULP3) regulates receptor trafficking in primary cilia and antagonizes SHH signaling. *Tulp3* knockout mice are embryonic lethal with developmental abnormalities in multiple organs, while tissue-specific knockouts and viable missense alleles cause polycystic kidney disease. Human patients with *TULP3* mutations present with variable, but often multi-organ fibrotic disease. We previously showed that mouse and human *Tulp3* expression is negatively regulated by ZNF423, which is required for SHH sensitivity in some progenitor cell models. The level of TULP3 function required to prevent mutant phenotypes has not been known. Here we report a *Tulp3* quantitative allelic series, designed by targeting the polypyrimidine tract 5' to the splice acceptor of a critical exon, that shows distinct dose-response effects on viability, brain overgrowth, weight gain, and cystic kidney disease. We find limited evidence for genetic interaction with *Zfp423* null or hypomorphic mutations. Together, these results establish an approach to developing quantitative allelic series by exon exclusion, rank-order dose-sensitivity of *Tulp3* phenotypes, and model thresholds for TULP3 function to prevent severe outcomes.

INTRODUCTION

TUB-like protein 3 (TULP3), like TUB, is a phosphatidylinositol-(4,5)-bisphosphate (PIP2) binding protein that is dynamically localized to different cell compartments, including plasma membrane, nucleus, and primary cilia, during G protein coupled receptor signaling [1, 2]. TUB and TULP3 are broadly expressed, close homologs [3] that promote trafficking of membrane proteins into primary cilia through interactions with phosphatidylinositol-(4,5)-bisphosphate (PIP2), the intraflagellar transport complex A (IFT-A), and cargoes–notably G protein-coupled receptors and polycystins [4-10]. TULP3 antagonizes SHH signaling through its trafficking activity [2, 4, 6, 11-13], with consequences for the development and function of several organ systems. We previously showed that *Tulp3* is a target of *Zfp423* in both mouse and human cells [14] and set out to test their genetic interaction *in situ*.

Mouse genetics identified functional requirements for *Tulp3* across several organs and cell types. *Tulp3* mutants from either ES-cell targeting or chemical mutagenesis showed embryonic lethality with exencephaly, spina bifida, preaxial polydactyly, splayed vertebrae, and increased SHH activity [2, 12, 15]. A subsequent viable missense allele, *Tulp3*^{K407I} (a.k.a. *Tulp3*^{m1Kflj}), and conditional deletion in either collecting ducts (*Tulp3*$^{tm1a(EUCOMM)Hmgu}$ with *Hoxb7*-Cre) or nephrons (with *Ksp*-Cre) both showed polycystic kidneys in embryos or young mice, while simultaneous deletions of *Tulp3* and the polycystin gene *Pkd1* suppressed the renal cysts seen in either single gene deletion [16, 17]. Despite this progress, the amount of *Tulp3* function required for viability and the dose-response for postnatal phenotypes have remained open questions and direct comparisons across alleles in different labs are complicated by use of different genetic backgrounds for each of these mutations.

Subsequent human studies identified biallelic damaging *TULP3* variants in patients with hepatic fibrosis, fibrocystic kidneys, cardiomyopathy, and compromised DNA damage response [18], which is a shared feature among several ciliopathy gene disorders [19-23]. Variants included frameshift, nonsense, splice variant, and amino acid substitutions in the highly conserved TUB domain. An additional patient reported later in ClinVar had a splice donor mutation after exon 7. Onset and progression were variable among affected individuals in the documented cohort, but liver and kidney damage preceded other organ involvement, with non-obstructive hypertrophic cardiomyopathy reported only in a minority of patients and only in the sixth decade or later. Typical for rare genetic disorders, how much of the variation in disease presentation is due to allelic differences and how much to other causes–and how much functional recovery would be required for benefit–are not known. Recent evidence has also implicated TULP3 in the effects of caloric restriction on aging [24].

Given high levels of genetic heterogeneity (both locus and allelic) and variable penetrance of disease phenotypes in human ciliopathies as well as differing genetic backgrounds and individualized phenotyping protocols in animal models, relatively few studies have isolated allele-specific effects from potential effects of genetic background and non-genetic factors. Fewer have done so with quantitative alleles that titrate levels of genetic activity at the subject locus. Here we develop a *Tulp3* quantitative allelic series in mice by editing the polypyrimidine tract adjacent to a frame-shifting exon (exon 7) to modulate exon inclusion and expression level, as well as qualitative variants lacking a conserved Tub-N domain (exon 4). We titrate clinically relevant phenotypes across this series and test prior hypotheses for genetic interaction between *Tulp3* and *Zfp423* mutations in mice. Our results establish a generalizable approach and show that minimal (≤5%) of TULP3 expression level is required for viability, that modest increments of expression improve clinically-related phenotypes, and that for at least one exon, loss of conserved protein segments has a comparatively modest impact on genetic function.

RESULTS

Quantitative allelic series by targeting inclusion of a frame-shifting exon.

We targeted two sites in *Tulp3* based on its exon structure and protein coding domains, using a high-fidelity Cas9 and a pool of donor oligonucleotides to template repair on a coisogenic FVB/NJ genetic background (Figure 1A). We generated two mutations at exon 4, which encodes a conserved protein domain, but whose skipping would maintain the open reading frame in the resulting mRNA (Figure 1B). Both mutations should abolish exon 4 inclusion in *Tulp3* mRNA but have residual genetic function unless the conserved Tub-N domain is essential to all TULP3 activities. We targeted the polypyrimidine tract 5' to *Tulp3* exon 7 splice acceptor to decrease the exon inclusion rate in processed mRNA. Exon 7 was selected based on its exclusion resulting in a reading frame shift, such that the rate of exon 7 inclusion should predict the degree of genetic function of an edited allele. We recovered seven distinct alleles from a single injection job, including all four templated by the oligonucleotide pool and three insertion/deletion (indel) variants, of which two (Δ5, Δ3) were predicted to abolish exon 7 inclusion and function as null mutations (Figure 1C). Oligonucleotide donors for editing and assay primers are given in S1 and S2 Tables.

RT-PCR assays show that the exon 7 mutations result in reduced exon 7 utilization. Exon inclusion assays showed inclusion rates that quantitatively distinguished alleles (Figure 1D). The non-templated 4-bp insertion allele (i4) predicted a strong alternative splice acceptor that would produce a frameshift without inducing exon skipping. DNA sequencing of the RT-PCR product from an *i4* homozygote of steady-state *Tulp3* RNA is spliced into this upstream decoy site rather than the in-frame splice acceptor (Figure 1E).

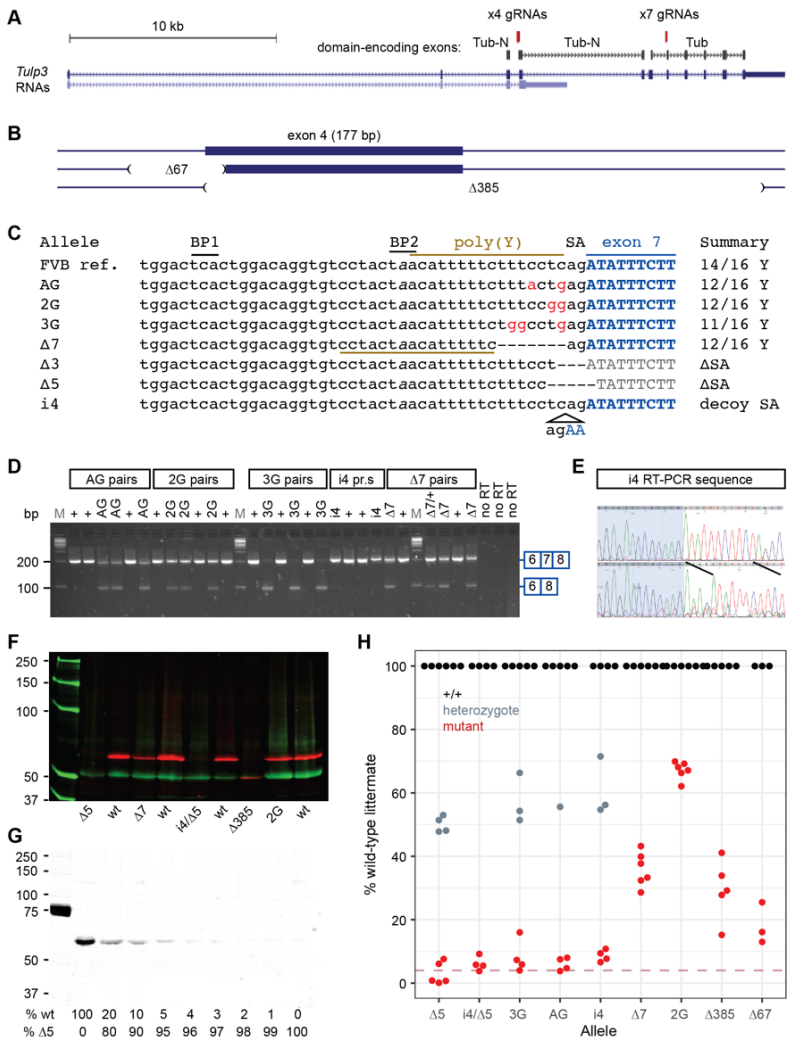

Figure 1. Allelic series targeting polypyrimidine tracts. (**A**) Genomic organization of *Tulp3* showing targeted exons relative to encoded domains. (**B**) Deletion alleles relative to exon 4. (**C**) Exon 7 alleles relative to FVB/NJ reference sequence. BP, splicing branch points; SA, splice acceptor; poly(Y), polypyrimidine tract. (**D**) RT-PCR shows allele-dependent levels of exon skipping induced by mutations in the polypyrimidine tract 5' to exon 7. (**E**) Sanger sequence of a control (top) and *i4* homozygote (bottom) shows a majority of steady-state RNA spliced into the mutant-specific decoy splice acceptor. (**F**) Two-color Western blot detects TULP3 (red, upper) and loading control (green, lower) relative to size marker (kD). (**G**) Null (Δ5/Δ5) protein extracts with wild-type spike-in estimates detection limit at ~4% of control. (**H**)

Band intensities relative to littermate controls define a quantitative allelic series based on reduced TULP3 protein expression. Dashed line, 4%.

Western blots confirmed and quantified reductions in TULP3 protein expression across the allelic series. Extracts from E14.5 embryo littermate pairs showed reduced expression of otherwise wild-type TULP3 protein from each of the exon 7 alleles, with a reduced steady-state amount of a smaller TULP3 protein from the exon 4-skipping alleles (Figure 1F). Spike-in controls showed a detection limit at ~4% of wild-type levels under our conditions (Figure 1G). The very low levels achieved by splicing variants and null heterozygote expression at 50% suggest little to no compensatory feedback regulation for TULP3 levels. The lowest expression genotype, i4/Δ5 compound heterozygotes, expressed ≤5% of wild-type littermate TULP3 levels (Figure 1H and S3_Table). These results demonstrate simple construction of a quantitative allelic series that can be used for calibrating genetic function relative to *TULP3* phenotypes or potential interventions, using an approach that should be generalizable to other genes.

Minimal TULP3 is required for survival to adulthood.

Having a quantitative allelic series on a coisogenic background allowed us to estimate the amount of *Tulp3* genetic function required to escape lethality and other major phenotypes. The Δ5 splice acceptor mutation behaved as a genetic null. Homozygous Δ5 embryos produced no detectable TULP3 protein and showed brain overgrowth resulting in exencephaly and preaxial polydactyly resulting in supernumerary digits by E14.5 (Figure 2A), consistent with previous knockout models on other strain backgrounds [2, 11, 12, 15]. Postnatally, we found no surviving homozygotes among ~200 progeny from null-allele heterozygote crosses (Figure 2B). By contrast, hypomorphic genotypes, including the i4/Δ5 allelic combination that expressed only ~5% of normal TULP3 levels showed no significant evidence for reduced viability in moderately large crosses. A nominal effect of the least severe allele, 2G, did not survive correction for family-wise error rate and included the caveat that allele-specific PCR assays for 2G, 3G, and

AG were tuned to avoid homozygote false-positives and therefore likely under-count true homozygotes. Pooling hypomorphic allele data from all length-specific assays (i4/Δ5, i4, Δ7, and the two exon 4 deletions) was not significant despite large aggregate sample (p=0.17, Chi-squared test). Littermate pairs selected for age-dependent phenotypes similarly failed to support a significant effect of hypomorphic genotypes on later survival. These results suggest that for severe *Tulp3* phenotypes, even small increments of improved function might be beneficial, with only ~5% of wild-type levels required for gestation and long-term survival.

A

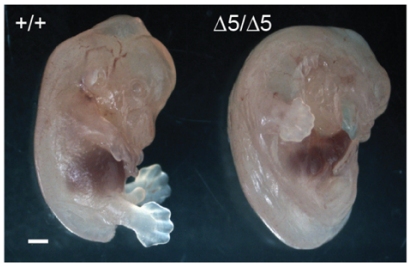

B

Allele	non-mut	mut	χ^2 p	FWER-adj p
Δ5	196	0	6.3×10^{-16}	6.3×10^{-15}
Δ3	134	0	2.3×10^{-11}	2.1×10^{-10}
i4/d5	228	69	0.48	0.92
3G	223	57	0.073	0.51
AG	263	73	0.17	0.75
i4	266	79	0.37	0.90
Δ7	113	34	0.60	0.92
2G	213	52	0.043	0.30
Δ67	358	105	0.25	0.80
Δ385	362	122	0.92	0.92

Figure 2. Minimal TULP3 expression is sufficient for viability and survival to adulthood. (**A**) Exencephaly and polydactyly are evident by E14.5 in Δ5 homozygotes. Bar, 1 mm. (**B**) Genotype ratios show complete lethality of null animals, but no significant evidence for reduced viability among even the strongest hypomorphic genotypes with TULP3 expression near the limit of detection in Western blots. Nominal p-values from the 1-df chi-squared test were adjusted for family-wise error rate (FWER-adj p) using Hommel's method [25].

Hypomorphic *Tulp3* genotypes gain excess weight.

From littermate pairs left during several months of the COVID-19 pandemic, *Tulp3* hypomorphic mutants were visibly obese relative to co-housed same-sex littermates (Figure 3A and S4_Table). As a more quantitative test and to determine the time course for onset, we followed co-housed, same-sex littermate mutant-control pairs with periodic weight measurements in a subsequent cohort from weaning to >6 months. For the lowest TULP3-expressing genotype

(i4/Δ5), a clear trend showed increasing weight gain over time by mutants relative to their littermate controls for both sexes (Figure 3B). Results from other mutants showed similar though less pronounced trends, roughly proportional to expression level and loss of exon 4 (Figure 3C). As some littermate pairs were censored at later times due to age-related health issues independent of genotype, we examined pairs weighed at 100-132 days postnatal (Figure 3D). While modest sample sizes and corrections for family-wise error rate limited power for individual genotypes, aggregating variants whose effect on TULP3 expression was relatively weak (2G, Δ5/+, and Δ7), weak but included removal of exon 4 (Δ67, Δ385), or relatively strong (i4, AG, 3G) showed a rough correlation between weight gain and TULP3 expression loss. We saw significant effects of all but the weak alleles, with exon 4 alleles roughly comparable to strong alleles, and with the i4/Δ5 combination having a stronger effect than all others. These data show a quantitative effect of TULP3 expression level on weight homeostasis at levels below 30% of wild-type.

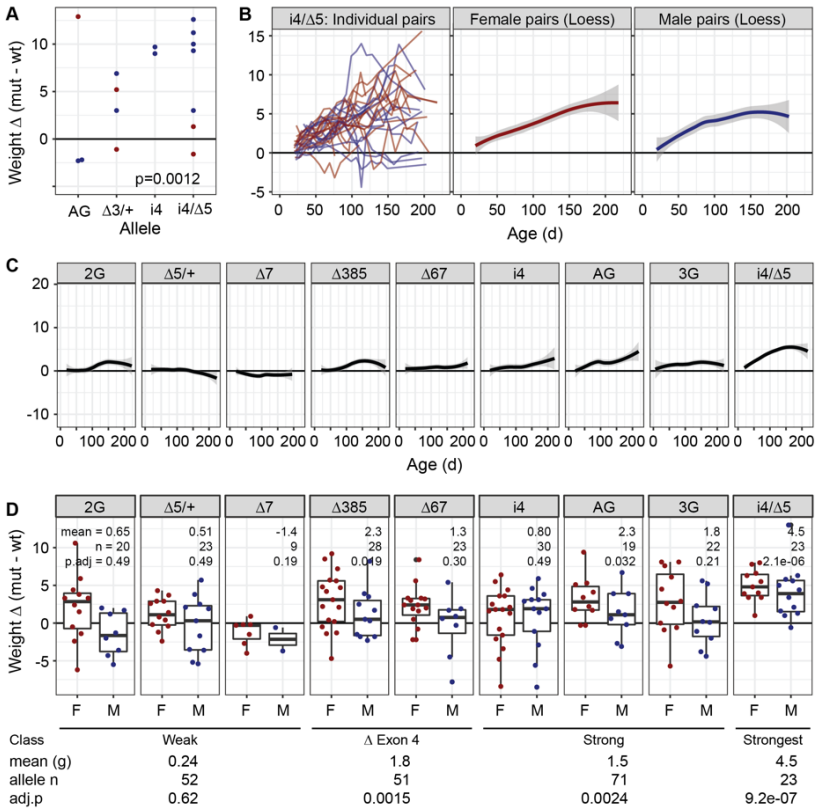

Figure 3. Allele-dependent weight gain in *Tulp3* hypomorphs. (**A**) Incidental observation of co-housed sex-matched littermates showed obesity in aged *Tulp3* mutants. Each point is the difference (mutant-wildtype) in grams for a littermate pair. Mean age 220 days. (**B**) Time course of weight difference in individual i4/Δ5 littermate pairs and loess regression plots of i4/Δ5 pairs for each sex. (**C**) Loess plots for each allele, both sexes. (**D**) Summary boxplots with points for distinct individual pairs (first measure after postnatal day 100) for each *Tulp3* allele. Mean difference in grams, sample size, and FWER-corrected p-values from paired sample t-tests are given for each allele (above) and expression class (below).

Strongest reduction in *Tulp3* produces increases in brain measures.

Tulp3 knockout mice, including Δ5 allele homozygote reported here, display multisystem disorders including exencephaly secondary to brain overgrowth (Figure 4 and S5_Table). To determine whether viable *Tulp3*-mutant mice display related changes to gross brain morphology, we adopted a pipeline of 8 simple measures (vermis width, cerebellar hemisphere anterior-posterior distance, and maximum brain width from dorsal photographs of whole brain; vermis sagittal area, cortical thickness, corpus callosum thickness, and anterior commissure thickness from block face preparation photographs) that we previously used for analysis of *Zfp423* allelic variants [26]. We found that i4/Δ5 compound heterozygotes, the most severe viable genotype with respect to TULP3 protein level, had increased vermis sagittal area and cerebellar hemisphere anterior-posterior distance (4.5-6.0%) after correction for multiple outcome measures, with nominal support for increased brain width (2.6%), relative to same-sex littermate controls (Figure 4). Pooled data from the next most severe genotypes (i4/i4, AG/AG,

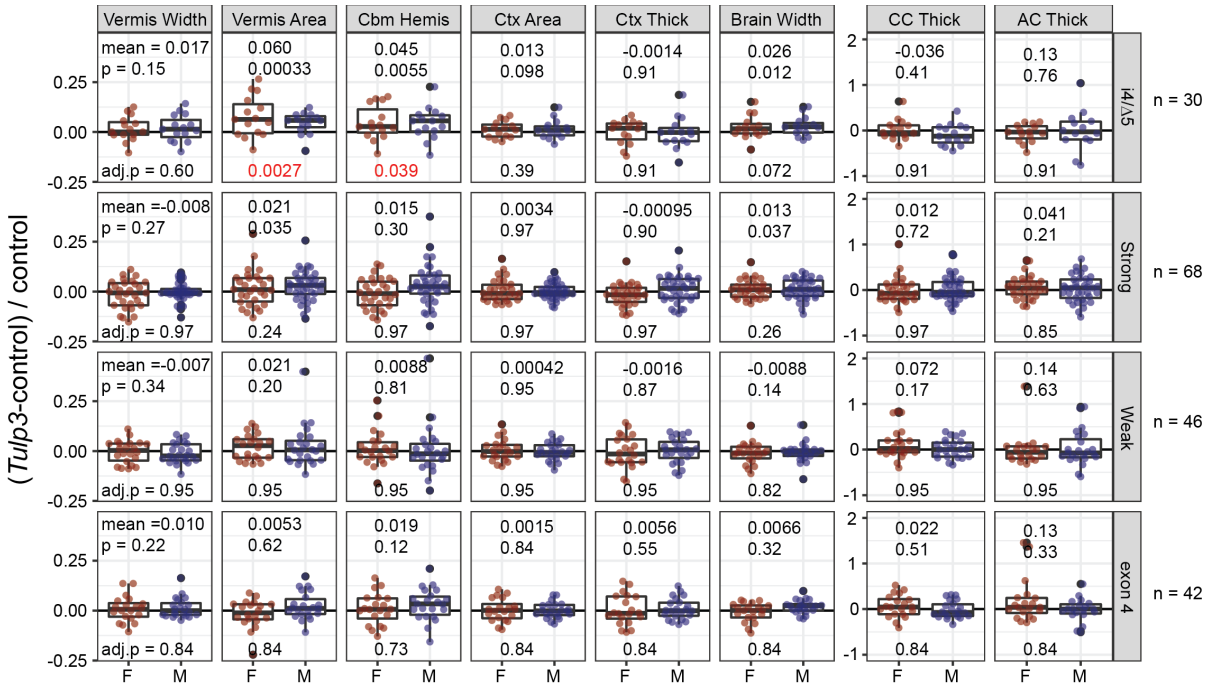

Figure 4. The strongest viable *Tulp3* variants influence brain morphology. (**A**) Compound heterozygotes i4/Δ5 average ~5-6% larger cerebellar vermis sagittal areas and anterior-posterior dimension of the cerebellar hemispheres. The widest extent of the brain was also nominally larger, but did not survive correction for multiple phenotypes (top row). Other strong hypomorphic genotypes (i4/i4, 3G/3G, AG/AG; combined to improve power across a similar expression level) showed nominal support for a lesser increase in vermis area and brain width that did not survive correction (second row). Neither the weaker exon 7 alleles (2G and Δ7) nor the exon 4 deletions (Δ67, Δ385) returned even nominally significant results for any measure. Mean, nominal p-value (paired sample t or Wilcoxon signed rank test), and adjusted p-value after FWER correction across 8 phenotype measures are shown. Abbreviations: Cbm Hemis, anterior-posterior dimension of the cerebellar hemispheres; Ctx Area, cortical area in dorsal surface view; Ctx Thick, average cortical thickness at 15°, 30°, and 45° from midline in coronal block face view; CC and AC Thick, thickness of the corpus callosum and anterior commissure, respectively, at the midline.

and 3G/3G) showed nominal increases in vermis area and brain width (1.3-2.1%) that did not survive correction for multiple tests. These data show that even viable reduction in TULP3 can result in modest brain overgrowth phenotypes and reinforce the conclusion that even modest increases in *Tulp3* function can significantly impact phenotypic outcomes.

Progressive kidney cystogenesis responds to small increments of TULP3 expression. *Tulp3* tissue-specific knockouts and a viable missense variant had cystic kidney disease, but neither the time course of disease nor the quantitative level of gene function to reduce or ameliorate primary endpoints have been known. We quantified a cystic index for sectioned kidneys from same-sex littermate pairs across a range of ages for each *Tulp3* allele using CystAnalyzer [27] (Figure 5 and S6_Table). The presence and size of cysts in aged animals visibly varied across alleles (Figure 5A). Cysts were evident for each of the strong exon 7 alleles but less frequent or not evident for weaker alleles that expressed ≥30% of control levels of TULP3 (Figure 1G). The two exon 4 deletion/skipping alleles combined showed a reproducibly low level of cysts, consistent with the relatively low steady-state protein level we observed, but not consistent with exon 4 encoding an essential function. The extent of cystogenesis for each genotype inversely correlated with expression level and increased with age (Figure 5B). In a two-factor ANOVA model, genotype ($p = 7.5 \times 10^{-7}$) and age ($p = 0.043$) were significant, with significant pairwise differences between i4/Δ5 and all others ($p < 1 \times 10^{-2}$), and between i4 and 3G ($p = 0.034$) or weaker alleles, but i4 and AG were not statistically different ($p > 0.99$). These data support a continuous relationship between kidney health and TULP3 expression below 50%, with particularly steep dose-response effects below ~10% of control levels.

Despite evident tissue damage, veterinary blood chemistries from aged littermate pairs (minimum 119 days, mean 234) did not detect differences in standard measures across 16 sample pairs from strong hypomorphic alleles (Supplemental Figure S1_Figure and S7_Table).

This suggests that histological measures may be more sensitive than standard blood chemistries for modeling ciliopathy defects in mice.

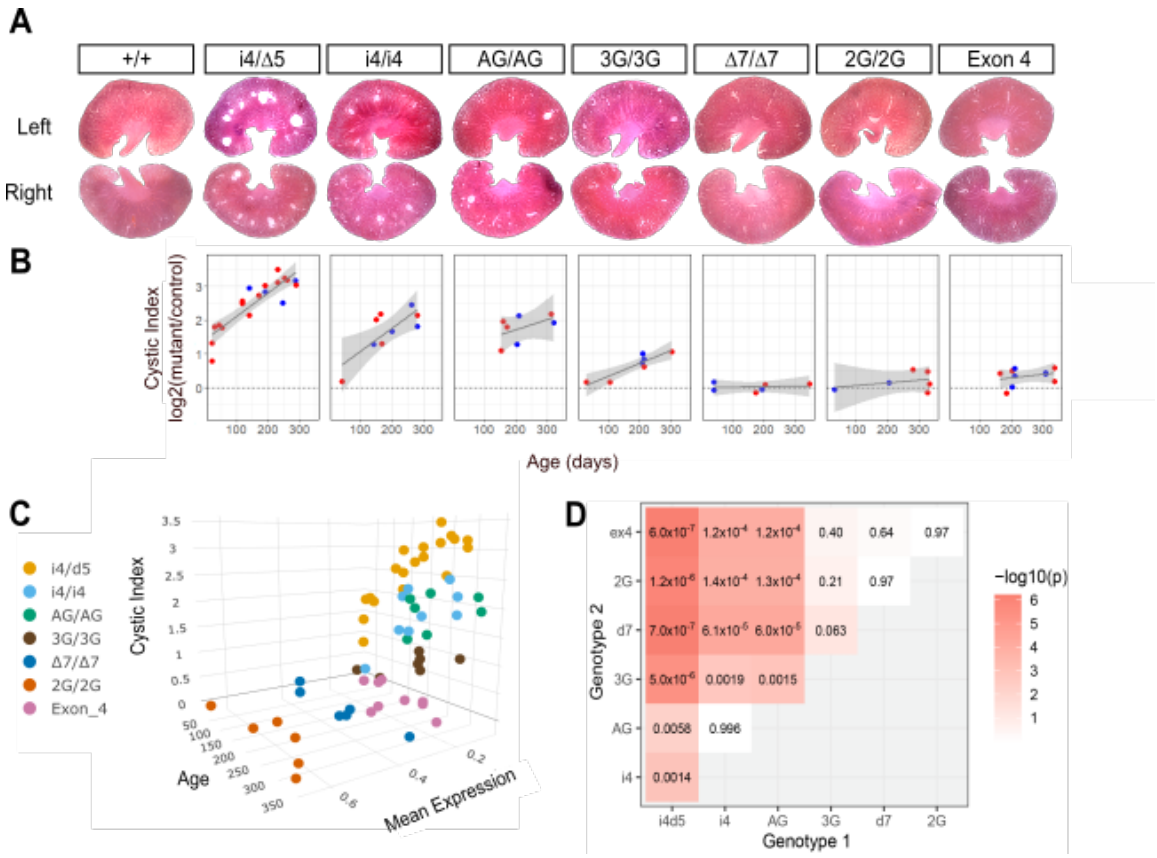

Figure 5. Allelic series shows dose-response in kidney cystogenesis. (**A**) Kidney sections from aged adult mice show allele-typical degrees of cystogenesis. (**B**) Cystic index for *Tulp3* variants showed allele- and age-dependence relative to same-sex control littermates. A generalized linear fit and 95% confidence interval are shown. (**C**) Three-dimensional visualization illustrates a sharp shift in cystic index across TULP3 expression levels. (**D**) Heatmap with printed values for TukeyHSD post-hoc test for difference between genotypes after two-factor ANOVA for cystic index as a function of genotype and age.

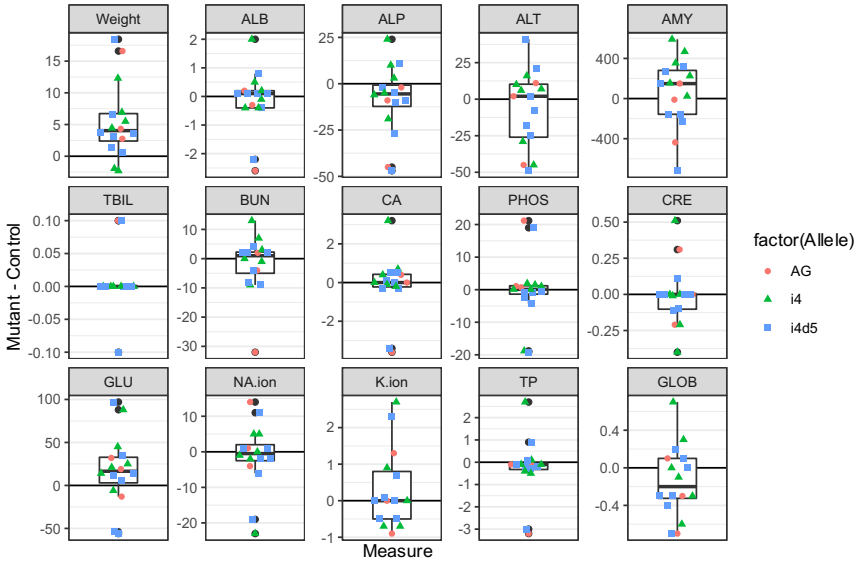

Supplemental Figure S1. No striking differences in blood chemistries among 16 sex-matched littermate pairs. Standard blood chemistry panels from same-sex littermate pairs from strong *Tulp3* allele combinations found no consistent differences dependent on genotype, in contrast to their body weights, which confirmed the differences shown in Figure 3.

***Tulp3* reduction does not suppress major *Zfp423* brain phenotypes.**

We previously showed that *TULP3/Tulp3* is a repressive target of the ZNF423 (mouse ZFP423) transcription factor in both mouse granule cell progenitors and a human medulloblastoma (DAOY) cell line and that simultaneous knockdown of both genes reversed a SMO translocation defect of *ZNF423* knockdown in DAOY cells [14]. To test whether germline mutations that decrease *Tulp3* level suppress *Zfp423* developmental phenotypes at an anatomical level, we crossed *Zfp423* null as well as two ZFP423 domain-specific mutations to the *Tulp3*-i4/Δ5 combination, in a coisogenic FVB/NJ background and measured weight and eight neuroanatomical parameters that we previously used to quantify a *Zfp423* allelic series [26] (Figure 6).

We first compared *Zfp423*-null mutants (N515Tfs*43, also known as N507Tfs*43 or *Zfp423*^{em5Haml}) with or without strongly reduced *Tulp3* expression (Figure 6A and S8_Table). Because *Zfp423* null homozygotes have reduced viability, we compared sex-matched mutant-wildtype pairs between two crosses of *Zfp423* heterozygotes, one in which all animals were *Tulp3* wild-type and one in which parents were *Tulp3*-i4/Δ5, resulting in offspring that were either i4/Δ5 or i4/i4. In the latter cross, paired samples had the same *Tulp3* genotype. We then compared the means of pair-wise differences between the two crosses. While seven out of nine measures trended toward improvement in the double mutant, neither individual measures nor the overall trend met even nominal significance at conventional statistical thresholds. While these results did not rule out a minor effect of *Tulp3* on *Zfp423* null phenotypes, nor an effect on some cell-level phenotype, they did not support the hypothesized genetic suppressor activity at the level of *Zfp423* brain structural abnormalities.

We also examined the effect of *Tulp3* on two viable and fertile alleles of *Zfp423* (Figure 6B and S9_Table). *Zfp423* encodes 30 C2H2 zinc finger domains and an additional putative non-canonical 4-cysteine zinc finger [28], clusters of which mediate several known physical interactions [22, 29-32], including a C-terminal homophilic interaction domain and SMAD protein-interacting region in zinc fingers 14-19. Both a 210-bp in-frame deletion (Δ210) that eliminated the 4-cysteine zinc finger region in the homophilic interaction domain and a 261-bp deletion (Δ261) that fused the first half of zinc fingers 15 to the second half of zinc finger 18 in the SMAD-interacting region resulted in quantifiable defects in weight and brain measures [26]. We used crosses in which both parents were homozygous for one of these two *Zfp423* domain deletions and heterozygous for *Tulp3*-i4 in one parent and *Tulp3*-Δ5 in the other to produce same-sex littermate pairs of *Zfp423* hypomorphs that are *Tulp3* wild-type or i4/Δ5. We observed nominal improvements in weight, anterior-posterior distance in cerebellar hemispheres, and thickness of the corpus callosum, but each effect had small magnitude and only weight survived

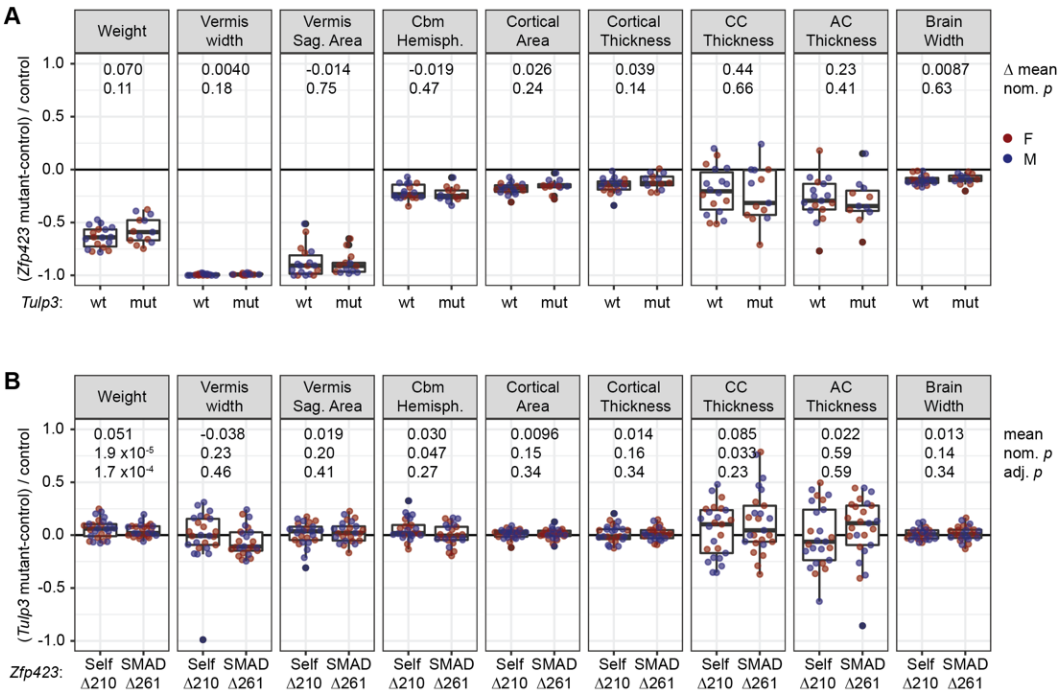

Figure 6. Genetic reduction of *Tulp3* does not suppress *Zfp423* null or hypomorphic phenotypes. (**A**) Major *Zfp423*-null phenotypes are not substantially improved by reduced *Tulp3* expression. Each point represents a *Zfp423* mutant-wildtype same-sex littermate pair, from crosses with *Zfp423*^{N507Tfs*43} heterozygous and either *Tulp3* wild-type (wt, n=18), or *Tulp3* i4/Δ5 (mut, n=13) parents. Differences in the means between *Zfp423* and double mutants along with nominal *p*-values from Welch Two Sample t-test are given. (**B**) *Tulp3* reduction had only nominal effects on *Zfp423* hypomorph measures other than weight. Homozygotes for viable in-frame deletions of a self-association domain (Δ210) or SMAD-binding zinc fingers (Δ261) with viable reductions in *Tulp3* (i4/Δ5 or i4/i4) were compared to same-sex littermates homozygous for the same *Zfp423* mutation but wild-type for *Tulp3*. Self-association domain n=26 pairs, SMAD-binding domain n=25 pairs. Paired sample t-tests or Wilcoxon signed rank test (vermis width) before and after adjustment for family-wise error rate (Hommel's method) are shown for the combined sample (n=51). Effects on weight were independently significant in each group.

correction for family-wise error rate across the nine measures. These results suggest that *Tulp3* reduction may have had a suppressing effect on some *Zfp423* anatomical phenotypes in hypomorphic variants, but that any effect sizes were quite small relative to the *Zfp423* main effects.

DISCUSSION

Here we demonstrated a simple method for creating a quantitative allelic series in mice and identified distinct TULP3 levels required for viability, neuroanatomical measures, kidney homeostasis, and obesity and used that series to calibrate a qualitative allele affecting both expression level and protein composition. These results provide a generalizable strategy for efficient quantitative animal models of genetic disorders and identify new features of *Tulp3* pathology in mice.

From a single “one-pot” CRISPR/Cas9 editing experiment at exon 7, we recovered 6 functionally distinct alleles (counting only one of two presumptive nulls, Figure 1) targeting the polypyrimidine tract adjacent to an essential, frame-shifting exon. Null variants recapitulated expected embryonic lethal phenotypes, including polydactyly and exencephaly, while other recovered alleles that reduced *Tulp3* RNA and protein expression showed a range of phenotypes that correlated with reduction in expression level. Our approach should be extensible to other genes, though details may vary with the strength of cis-acting signals for exon inclusion. This approach allows more accurate modeling of pathogenic variants by calibrating the amount of genetic function required for measured phenotypes with much more precision than simple null and heterozygote collections in large-scale phenotyping centers.

Our results support different quantitative requirements for TULP3 among affected tissues. Measures across calibrated *Tulp3* genotypes allowed us to assess quantitative thresholds and dose-responses for several notable phenotypes (Figure 7). The data showed a low threshold (~5% of control) to allow viability while avoiding polydactyly and severe neural tube defects, although the strongest viable genotype had measurable if slight increases in some morphological brain measures. Among viable genotypes, we found significant excess weight relative to littermates that expressed less than one-third of control TULP3 levels, with a slightly larger impact of exon 4 deletion relative to its measured expression level. Notably, we found later onset and less severe kidney phenotypes for viable *Tulp3* variant combinations in our FVB-coisogenic models than previous reports from mice on C57BL/6 or mixed backgrounds, despite inclusion of very strong reductions in TULP3 expression level. These differences may include effects of genetic modifiers, but we note that presumptive null variants on FVB recapitulate prior phenotypes. This suggests that substitution variants with highly cystic kidneys by birth, such as K407I [33], represent severe loss of function. Further studies will be required to determine whether these differences indicate strain-dependent genetic modifiers or environmental differences. Our data also showed that kidney cystogenesis had a quantitative dose-response to TULP3 level across a range from ~5-30% of control levels. Notably, this is a range that is not addressed in large consortia that assess knockout and heterozygote models. These data provide a unique quantitative framework for modeling human *TULP3* effects in mice with a generalizable approach and for estimating quantitative effects of qualitative protein variants.

	Δ5/Δ5	i4/Δ5	i4/i4	AG/AG	3G/3G	exon 4	Δ7/Δ7	2G/2G
Protein expression	0.03 ±.03	0.06 ±.02	0.08 ±.02	0.06 ±.02	0.08 ±.05	0.25 ±.10	0.36 ±.05	0.67 ±.03
Lethality	100	0	0	0	0	0	0	0
Polydactyly	100	0	0	0	0	0	0	0
Brain morphology	Severe	Slight	0	0	0	0	0	0
Weight excess	nd	4.5 g	1.5 g	1.5 g	1.5 g	1.8 g	ns	ns
Kidney cysts	(Severe)	2.8	1.8	1.7	0.72	0.29	0.02	0.14

Figure 7. Summary of TULP3 expression-dependent effects. Heat map shows mean protein level in E14.5 embryo heads (top row, blue) inversely proportional to measured phenotypes (rows 2-6, red). Very low levels of TULP3 expression are sufficient to avoid lethality and polydactyly. Only the lowest viable expression level has residual brain morphological abnormalities relative to same-sex control littermates. Genotypes with less than ~36% TULP3 expression show increased weight gain, with average values relative to same-sex littermates at ~100 days shown. Cystic index in kidneys showed continuous graded response to TULP3; interpolated average at 200 days is shown; severity of the null inferred from embryonic and juvenile kidneys of earlier *Tulp3* models [16, 17]. nd, not determined; ns, no significant difference.

MATERIALS AND METHODS

Mice. FVB/NJ mice were purchased from The Jackson Laboratory. *Zfp423* mutant mice were previously reported [26] and maintained coisogenic on FVB/NJ. Mice were maintained in a specific pathogen free (SPF) facility on 12 h light, 12 h dark cycle in high-density racks with HEPA-filtered air and ad libitum access to water and food (LabDiet 5P06). All animal experiments were approved by the University of California San Diego Institutional Animal Care and Use Committee (UCSD-IACUC) under protocol S00219.

Germline editing. Genome editing was contemporaneous with and essentially as described by Deshpande et al. [26]. Briefly, FVB/NJ one-cell embryos were injected with pre-assembled editing mixes in IDTE (10 mM Tris, 0.1 mM EDTA, pH 8.0) and transplanted into pseudo-pregnant females in the UC San Diego Moores Cancer Center Transgenic Mouse Shared Resource facility. Editing mixes were formulated by annealing tracrRNA and crRNA for ~30 minutes in IDTE or 0.5x duplex buffer (0.5x is 15 mM HEPES, pH 7.5; 50 mM potassium acetate), incubating with diluted Cas9 for 5 minutes (exon 4) or HiFi Cas9 for 15 minutes (exon 7), diluting the resulting complex in IDTE, and supplementing with oligonucleotide pools (Ultramers) as donors for homology-dependent repair. Diluted editing mixes as injected contained 1.2 to 1.5 μM crRNA:tracrRNA, 30 ng/μl Cas9 or HiFi Cas9, and 2.4 to 3.2 μM pooled Ultramer oligonucleotides. Targeting sequences for each crRNA, with protospacer-adjacent motif (PAM, in parentheses), were: CAGCTGGACCGTCGATGCCT (AGG) and TAGGAGCACATCCCCGCAAC (CGG) for exon 4 and CCGGCTAGAAGAAATATCTG (AGG) for exon 7. Ultramer oligonucleotide sequences are given in Supplemental Table S1. All editing components were purchased from Integrated DNA Technologies (IDT). Tail biopsy DNAs from potential founder (G0) animals were used for PCR-based sequencing using primers in Supplemental Table S2. Edited lines were maintained coisogenic by serial backcross to

FVB/NJ. Genotypes for stock maintenance and experimental subjects were determined by PCR assays (Supplemental Table S2). Nucleotide substitution allele (2G, 3G, and AG) used bidirectional-PCR amplification of specific alleles (biPASA) assay designs [34] unique to each allele.

RT-PCR. RNA was extracted with Trizol reagent from E14.5 embryo heads and reverse transcribed with SuperScriptIII (Invitrogen). Exon inclusion assays used 35 cycles of PCR with primers in flanking exons (Supplemental Table S2) and resulting products resolved by gel electrophoresis.

Western blots. Staged embryos were obtained by timed mating after 5 pm, with noon of the following day designated E0.5. Protein extracts from E14.5 heads were prepared in RIPA buffer (Teknova, R3792) supplemented with protease inhibitors (Sigma-Aldrich, P8340) from mutant and control littermate samples were separated in 13% acrylamide gels and electrophoretically transferred to nitrocellulose membranes (GVS, 1212590). After blocking in 5% non-fat dry milk (APEX, 20-241), membranes were exposed to rabbit anti-TULP3 ([2], gift of Dr. Jonathan Eggenschwiler) anti-phosphoprotein antibodies as a loading control (MilliporeSigma, P3300, P3430, P3555) followed by IR-680 conjugated donkey anti-mouse (LiCOR 926-68072) and IR-800 conjugated donkey anti-rabbit (LiCOR 926-32213) secondary antibodies. After washing 3x in TBST (20 mM Tris, 150 mM NaCl, 0.1% Triton X-100) retained antibodies were imaged on a LI-COR Odyssey imaging station and bands quantified using ImageStudio software (LiCOR).

Anatomical measures. Sequential, paired samples were weighed ~weekly for up 300 days. A small number of animals, predominantly females, developed circling behavior independent of genotype and were removed from the study. Simple brain morphological measures were made as described for *Zfp423* mutants [26]. Briefly, anesthetized mice were perfused with phosphate

buffer followed by 4% paraformaldehyde. Brains were removed and post-fixed in 4% paraformaldehyde at 4°C overnight. External dorsal and block face coronal and sagittal images were captured on a Zeiss stereoscope with a Nikon Ds-Fi1 camera and measurements made in ImageJ software [35]. Kidneys were post-fixed in 4% paraformaldehyde overnight, then cryoprotected in 20% sucrose, 1X PBS, 0.5 mM EDTA. Tissues were embedded in O.C.T. compound (Fisher Scientific, 23-730-571) and flash frozen using 2-methylbutane cooled on dry ice. 15 µm sections were cut using a Leica CM3050S Cryostat at -20°C. After staining with hematoxylin and eosin, sections were photographed and cystic index was measured using CystAnalyzer software [27] using a 10 µm diameter setting.

Statistical analyses. Data were visualized using ggplot2 with the ggbeeswarm package [36]. Data were assessed for normality using the Shapiro-Wilk test and evaluated for differences between same-sex littermates of opposite genotype using either parametric (t-test) or nonparametric (Wilcoxon signed rank test) for paired samples. Resulting nominal p-values were corrected for family-wise error rate (FWER) across phenotypes using Hommel's method [25]. All statistical tests were performed in R.

Ethics statement

All animal experiments were approved by the University of California San Diego Institutional Animal Care and Use Committee (UCSD-IACUC) under protocol S00291.

ACKNOWLEDGEMENTS

We thank Dr. Jonathan Eggenschwiler for the gift of TULP3 antibody. We thank Ella Kothari and Jun Zhao for mouse zygote injections performed in the UCSD Moores Cancer Center Transgenic Mouse Core Facility. We thank Oliver Zhang for genotyping assistance and reading the draft manuscript.

DATA AVAILABILITY

All graphical summary plots show individual measures as dots. Underlying tabular data are in supporting tables formatted as data frames.

FUNDING

This work was supported by grant R01 NS097534 from the National Institute of Neurological Disorders and Stroke to BAH. CAM was supported in part by a training grant from the National Cancer Institute, T32 CA067754. RZL was supported in part by an institutional grant from the National Institute of General Medical Sciences, R25 GM083275. The UC San Diego Transgenic Mouse Core is supported by NIH P30 CA023100 and P30 DK063491. The funders had no role in study design, data collection and analysis, decision to publish, or preparation of the manuscript.

COMPETING INTERESTS

The authors have declared that no competing interests exist.

REFERENCES

1. Santagata, S., et al., *G-protein signaling through tubby proteins.* Science, 2001. **292**(5524): p. 2041-50.
2. Norman, R.X., et al., *Tubby-like protein 3 (TULP3) regulates patterning in the mouse embryo through inhibition of Hedgehog signaling.* Hum Mol Genet, 2009. **18**(10): p. 1740-54.
3. Nishina, P.M., et al., *Molecular characterization of a novel tubby gene family member, TULP3, in mouse and humans.* Genomics, 1998. **54**(2): p. 215-20.
4. Mukhopadhyay, S., et al., *TULP3 bridges the IFT-A complex and membrane phosphoinositides to promote trafficking of G protein-coupled receptors into primary cilia.* Genes Dev, 2010. **24**(19): p. 2180-93.
5. Mukhopadhyay, S., et al., *The ciliary G-protein-coupled receptor Gpr161 negatively regulates the Sonic hedgehog pathway via cAMP signaling.* Cell, 2013. **152**(1-2): p. 210-23.
6. Chávez, M., et al., *Modulation of Ciliary Phosphoinositide Content Regulates Trafficking and Sonic Hedgehog Signaling Output.* Dev Cell, 2015. **34**(3): p. 338-50.
7. Garcia-Gonzalo, F.R., et al., *Phosphoinositides Regulate Ciliary Protein Trafficking to Modulate Hedgehog Signaling.* Dev Cell, 2015. **34**(4): p. 400-409.
8. Badgandi, H.B., et al., *Tubby family proteins are adapters for ciliary trafficking of integral membrane proteins.* J Cell Biol, 2017. **216**(3): p. 743-760.
9. Palicharla, V.R., et al., *Interactions between TULP3 tubby domain and ARL13B amphipathic helix promote lipidated protein transport to cilia.* Mol Biol Cell, 2023. **34**(3): p. ar18.
10. Palicharla, V.R., et al., *A defined tubby domain beta-barrel surface region of TULP3 mediates ciliary trafficking of diverse cargoes.* Mol Biol Cell, 2025. **36**(1): p. ar1.

11. Cameron, D.A., T. Pennimpede, and M. Petkovich, *Tulp3 is a critical repressor of mouse hedgehog signaling.* Dev Dyn, 2009. **238**(5): p. 1140-9.

12. Patterson, V.L., et al., *Mouse hitchhiker mutants have spina bifida, dorso-ventral patterning defects and polydactyly: identification of Tulp3 as a novel negative regulator of the Sonic hedgehog pathway.* Hum Mol Genet, 2009. **18**(10): p. 1719-39.

13. Mukhopadhyay, S. and P.K. Jackson, *The tubby family proteins.* Genome Biol, 2011. **12**(6): p. 225.

14. Hong, C.J. and B.A. Hamilton, *Zfp423 Regulates Sonic Hedgehog Signaling via Primary Cilium Function.* PLoS Genet, 2016. **12**(10): p. e1006357.

15. Ikeda, A., et al., *Neural tube defects and neuroepithelial cell death in Tulp3 knockout mice.* Hum Mol Genet, 2001. **10**(12): p. 1325-34.

16. Hwang, S.H., et al., *Tulp3 Regulates Renal Cystogenesis by Trafficking of Cystoproteins to Cilia.* Curr Biol, 2019. **29**(5): p. 790-802.e5.

17. Legué, E. and K.F. Liem, Jr., *Tulp3 Is a Ciliary Trafficking Gene that Regulates Polycystic Kidney Disease.* Curr Biol, 2019. **29**(5): p. 803-812.e5.

18. Devane, J., et al., *Progressive liver, kidney, and heart degeneration in children and adults affected by TULP3 mutations.* Am J Hum Genet, 2022. **109**(5): p. 928-943.

19. Shaheen, R., et al., *POC1A truncation mutation causes a ciliopathy in humans characterized by primordial dwarfism.* Am J Hum Genet, 2012. **91**(2): p. 330-6.

20. Garaycoechea, J.I., C. Quinlan, and M.S. Luijsterburg, *Pathological consequences of DNA damage in the kidney.* Nat Rev Nephrol, 2023. **19**(4): p. 229-243.

21. Choi, H.J., et al., *NEK8 links the ATR-regulated replication stress response and S phase CDK activity to renal ciliopathies.* Mol Cell, 2013. **51**(4): p. 423-39.

22. Chaki, M., et al., *Exome capture reveals ZNF423 and CEP164 mutations, linking renal ciliopathies to DNA damage response signaling.* Cell, 2012. **150**(3): p. 533-48.

23. Airik, R., et al., *Renal-retinal ciliopathy gene Sdccag8 regulates DNA damage response signaling.* J Am Soc Nephrol, 2014. **25**(11): p. 2573-83.

24. Qu, Q., et al., *Lithocholic acid binds TULP3 to activate sirtuins and AMPK to slow down ageing.* Nature, 2024.

25. Hommel, G., *A stagewise rejective multiple test procedure based on a modified Bonferroni test.* Biometrika, 1988. **75**(2): p. 383-386.

26. Deshpande, O., et al., *ZNF423 patient variants, truncations, and in-frame deletions in mice define an allele-dependent range of midline brain abnormalities.* PLoS Genet, 2020. **16**(9): p. e1009017.

27. Cordido, A., et al., *CystAnalyser: A new software tool for the automatic detection and quantification of cysts in Polycystic Kidney and Liver Disease, and other cystic disorders.* PLoS Comput Biol, 2020. **16**(10): p. e1008337.

28. Hamilton, B.A., *ZNF423 orthologs are highly constrained in vertebrates but show domain-level plasticity across invertebrate lineages.* bioRxiv, 2020: p. 2020.03.09.984518.

29. Tsai, R.Y. and R.R. Reed, *Cloning and functional characterization of Roaz, a zinc finger protein that interacts with O/E-1 to regulate gene expression: implications for olfactory neuronal development.* J Neurosci, 1997. **17**(11): p. 4159-69.

30. Tsai, R.Y. and R.R. Reed, *Identification of DNA recognition sequences and protein interaction domains of the multiple-Zn-finger protein Roaz.* Mol Cell Biol, 1998. **18**(11): p. 6447-56.

31. Hata, A., et al., *OAZ uses distinct DNA- and protein-binding zinc fingers in separate BMP-Smad and Olf signaling pathways.* Cell, 2000. **100**(2): p. 229-40.

32. Lauberth, S.M. and M. Rauchman, *A conserved 12-amino acid motif in Sall1 recruits the nucleosome remodeling and deacetylase corepressor complex.* J Biol Chem, 2006. **281**(33): p. 23922-31.

33. Legué, E. and K.F. Liem, Jr., *Mutations in Ciliary Trafficking Genes affect Sonic Hedgehog-dependent Neural Tube Patterning Differentially along the Anterior-Posterior Axis.* Neuroscience, 2020. **450**: p. 3-14.

34. Liu, Q., et al., *Overlapping PCR for bidirectional PCR amplification of specific alleles: a rapid one-tube method for simultaneously differentiating homozygotes and heterozygotes.* Genome Res, 1997. **7**(4): p. 389-98.

35. Schneider, C.A., W.S. Rasband, and K.W. Eliceiri, *NIH Image to ImageJ: 25 years of image analysis.* Nat Methods, 2012. **9**(7): p. 671-5.

36. Wickham, H., *ggplot2: Elegant Graphics for Data Analysis*. 2016, New York: Springer-Verlag.